Supporting information

Formation of $PbCl_2$-type AHF (A = Ca, Sr, Ba) with Partial Anion Order at High Pressure

Yumi Tsuchiya,‡[a] Zefeng Wei,‡[a] Thibault Broux,[a] Cédric Tassel,[a] Hiroki Ubukata,[a] Yuuki Kitagawa,[b] Jumpei Ueda,[b] Setsuhisa Tanabe,[b] and Hiroshi Kageyama*[a]

a. Department of Energy and Hydrocarbon Chemistry, Graduate of School of Engineering, Kyoto University, Nishikyo-ku, Kyoto 615-8510, Japan.

b. Graduate School of Human and Environmental Studies, Kyoto University, Sakyo-ku, Kyoto 606-8501, Japan.

‡These authors contributed equally to the publication.

*Corresponding Author

Email: kage@scl.kyoto-u.ac.jp

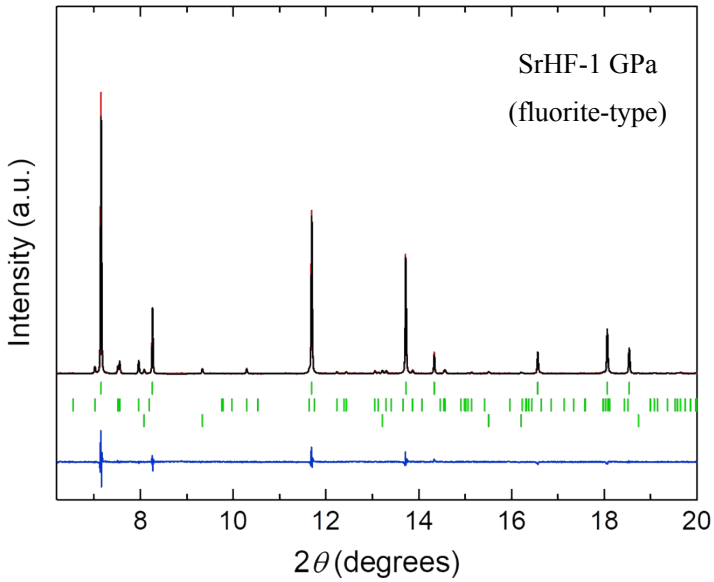

Figure S1. Rietveld refinement of SXRD data for SrHF synthesized at 1 GPa. The green ticks are SrH_2 (8.6%) and SrO (2.9%) as impurities.

Table S1. Structural parameters of SXRD data for fluorite-type SrHF synthesized at 1 GPa.

atom	Wyckoff position	*x*	*y*	*z*	B_{iso} (Å^2)	*g*
Sr	4*a*	0	0	0	0.80(1)	1[#]
H	8*c*	0.25	0.25	0.25	1.87(1)**	0.351*
F	8*c*	0.25	0.25	0.25	1.87(1)**	0.649*

Space group *Fm*-3*m*; *a* = 5.82849(3) Å,

R_p = 7.45%, R_{wp} = 9.28%

*sum constrained to be 1.

**constrained to be equal.

[#]fixed to be 1.

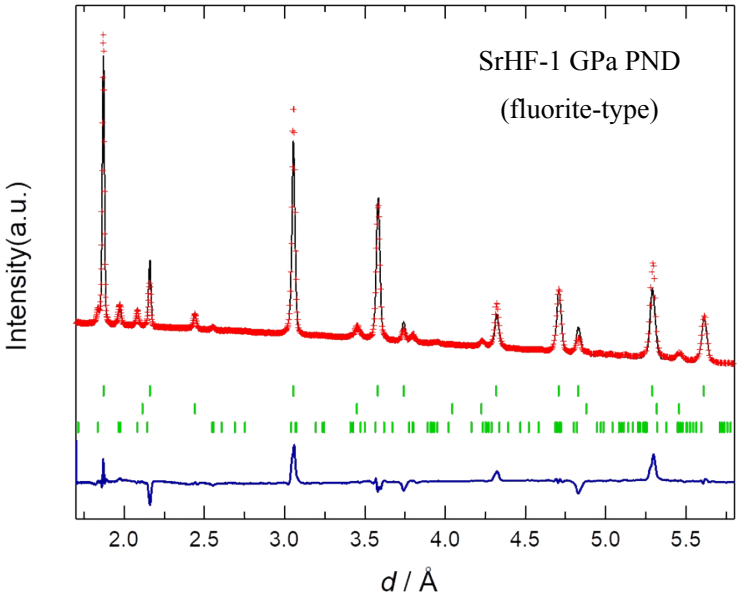

Figure S2. Rietveld refinement of PND data for SrHF synthesized at 1 GPa. The green ticks are SrH_2 (5.9%) and SrO (5.0%) as impurities.

Table S2. Structural parameters of PND data for fluorite-type SrHF synthesized at 1 GPa.

atom	Wyckoff position	*x*	*y*	*z*	B_{iso} (Å^2)	*g*
Sr	4*a*	0	0	0	0.517(1)	1[#]
H	8*c*	0.25	0.25	0.25	0.343(5)**	0.4892(1)*
F	8*c*	0.25	0.25	0.25	0.343(5)**	0.5107(1)*

Space group *Fm*-3*m*; *a* = 5.82879(1) Å,

R_p = 5.71%, R_{wp} = 6.97%

*sum constrained to be 1.

**constrained to be equal.

[#]fixed to be 1.

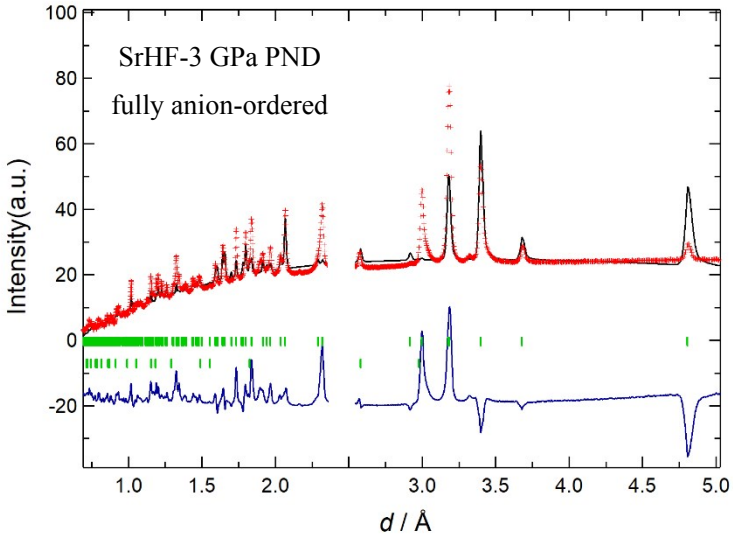

Figure S3. Rietveld refinement of PND data for $PbCl_2$-type SrHF synthesized at 3 GPa using the fully anion-ordered model (hydride anions exclusively occupy the square-pyramidal site).

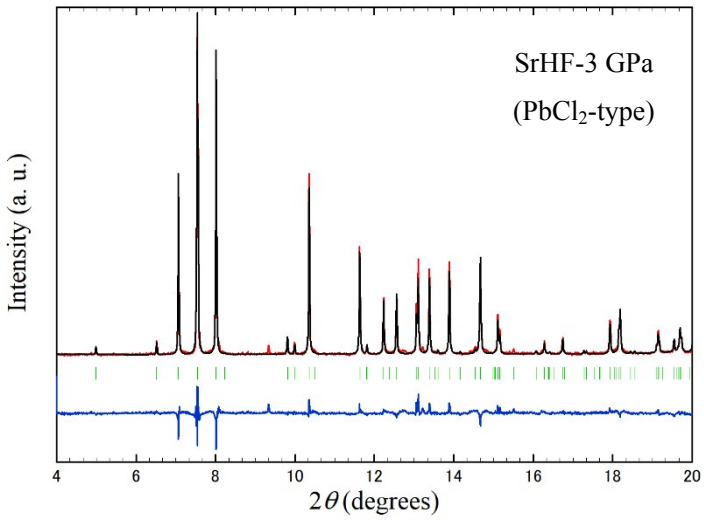

Figure S4. Rietveld refinement of SXRD data for SrHF synthesized at 3 GPa.

Table S3. Structural parameters of SXRD data for $PbCl_2$-type SrHF synthesized at 3 GPa.

atom	Wyckoff position	*x*	*y*	*z*	B_{iso} (Å^2)	*g*
Sr	4*c*	0.2435(3)	0.25	0.1115(2)	0.85	1$^{\#}$
H1	4*c*	0.3579(13)	0.25	0.4342(11)	1$^{\#}$	0.3
H2	4*c*	0.972(2)	0.25	0.6712(15)	1$^{\#}$	0.542
F1	4*c*	0.3579(13)	0.25	0.4342(11)	1$^{\#}$	0.7
F2	4*c*	0.972(2)	0.25	0.6712(15)	1$^{\#}$	0.458

Space group *Pnma*; a = 6.36768(11) Å, b = 3.83893(7) Å, c = 7.38450(13) Å,

R_p = 7.38%, R_{wp} = 9.27%

#fixed to be 1.

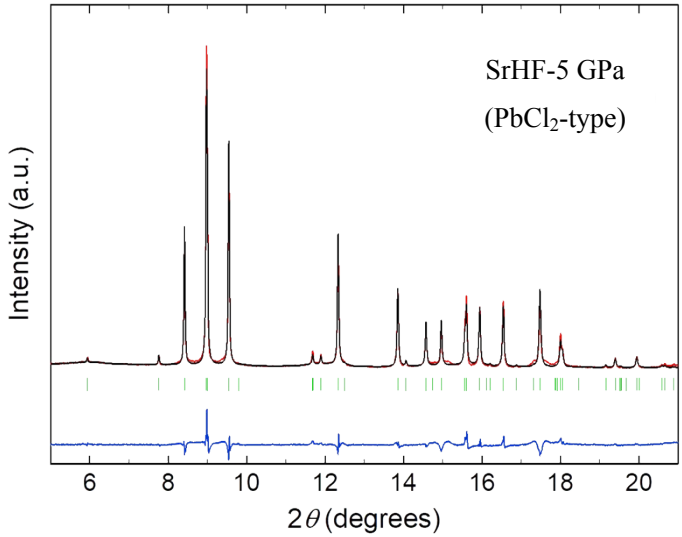

Figure S5. Rietveld refinement of SXRD data for SrHF synthesized at 5 GPa.

Table S4. Structural parameters of SXRD data for $PbCl_2$-type SrHF synthesized at 5 GPa.

atom	Wyckoff position	x	y	z	B_{iso} (Å^2)	g
Sr	4*c*	0.244(1)	0.25	0.1124(4)	0.94(7)	1#
H1	4*c*	0.355(4)	0.25	0.439(3)	1#	0.391(2)**
H2	4*c*	0.977(8)	0.25	0.677(5)	1#	0.609(2)**
F1	4*c*	0.355(4)	0.25	0.439(3)	1#	0.609(2)**
F2	4*c*	0.977(8)	0.25	0.677(5)	1#	0.391(2)**

Space group *Pnma*; a = 6.3757(4) Å, b = 3.8406(2) Å, c = 7.3889(5) Å,

R_p = 4.37%, R_{wp} = 6.03%

**sum constrained to be 1, respectively.

#fixed to be 1.

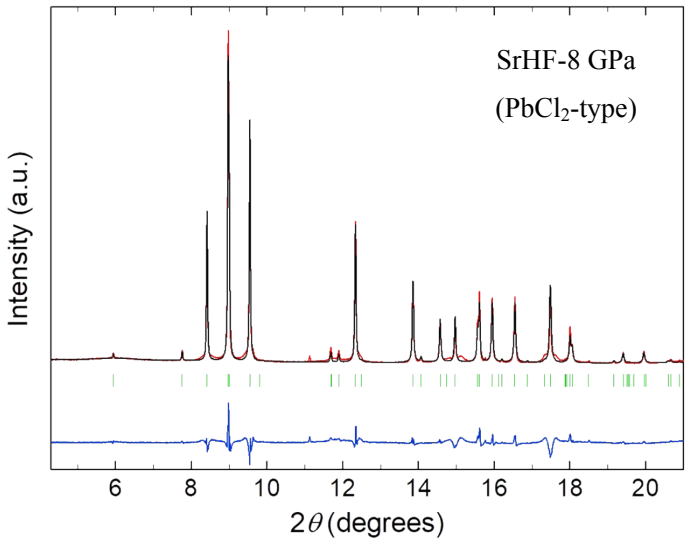

Figure S6. Rietveld refinement of SXRD data for SrHF synthesized at 8 GPa.

Table S5. Structural parameters of SXRD data for $PbCl_2$-type SrHF synthesized at 8 GPa.

atom	Wyckoff position	*x*	*y*	*z*	B_{iso} (Å^2)	*g*
Sr	4*c*	0.243(1)	0.25	0.1125(4)	0.74(6)	1$^{\#}$
H1	4*c*	0.355(3)	0.25	0.435(1)	1$^{\#}$	0.408(2)**
H2	4*c*	0.987(7)	0.25	0.680(1)	1$^{\#}$	0.592(2)**
F1	4*c*	0.355(3)	0.25	0.435(1)	1$^{\#}$	0.592(2)**
F2	4*c*	0.987(7)	0.25	0.680(1)	1$^{\#}$	0.408(2)**

Space group *Pnma*; a = 6.3739(3) Å, b = 3.8400(2) Å, c = 7.3895(4) Å,

R_p = 5.98%, R_{wp} = 8.03%

**sum constrained to be 1, respectively.

$^{\#}$fixed to be 1.

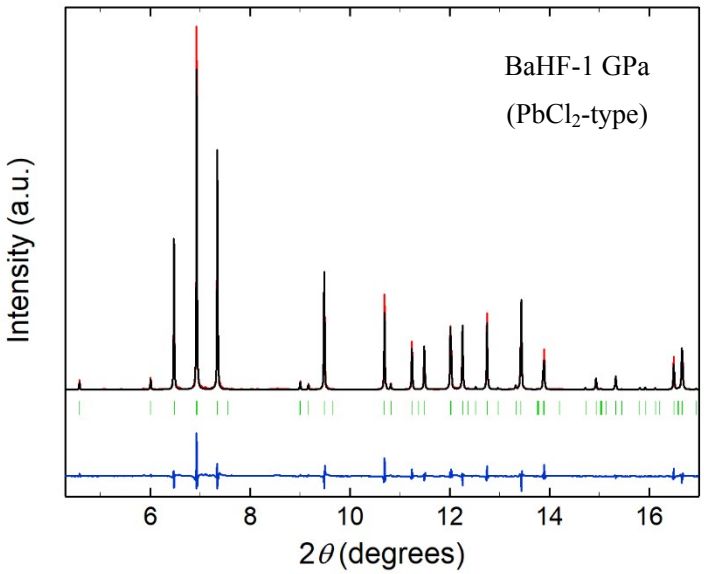

Figure S7. Rietveld refinement of SXRD data for BaHF synthesized at 1 GPa.

Table S6. Structural parameters of SXRD data for $PbCl_2$-type BaHF synthesized at 1 GPa.

atom	Wyckoff position	*x*	*y*	*z*	B_{iso} (Å^2)	*g*
Ba	4*c*	0.24067(16)	0.25	0.11263(10)	1.018 (15)	1[#]
H1	4*c*	0.3601(13)	0.25	0.43045(12)	0.79*	0.245**
H2	4*c*	0.983(4)	0.25	0.672(3)	0.47*	0.755**
F1	4c	0.3601(13)	0.25	0.43045(12)	0.79*	0.755**
F2	4c	0.983(4)	0.25	0.672(3)	0.47*	0.245**

Space group *Pnma*; a = 6.8578(7) Å, b = 4.12960(4) Å, c = 7.89038(8) Å,

R_p = 9.73%, R_{wp} = 12.5%

*fixed to be equal, respectively.

**sum constrained to be 1, respectively.

[#]fixed to be 1.

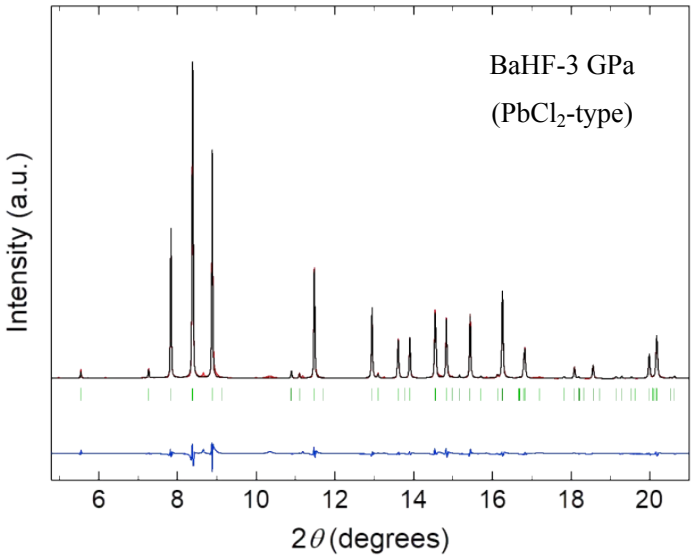

Figure S8. Rietveld refinement of SXRD data for BaHF synthesized at 3 GPa.

Table S7. Structural parameters of SXRD data for $PbCl_2$-type BaHF synthesized at 3 GPa.

atom	Wyckoff position	*x*	*y*	*z*	B_{iso} (Å^2)	*g*
Ba	4*c*	0.2411(2)	0.25	0.1126(1)	1.11(2)	1[#]
H1	4*c*	0.365(1)	0.25	0.425(1)	0.5(2)*	0.295(2)**
H2	4*c*	0.970(4)	0.25	0.669(3)	0.5(2)*	0.705(2)**
F1	4c	0.365(1)	0.25	0.425(1)	0.5(2)*	0.705(2)**
F2	4c	0.970(4)	0.25	0.669(3)	0.5(2)*	0.295(2)**

Space group *Pnma*; a = 6.8478(1) Å, b = 4.13198(6) Å, c = 7.8892(1) Å,

R_p = 6.75%, R_{wp} = 10.6%

*fixed to be equal, respectively.

**sum constrained to be 1, respectively.

[#]fixed to be 1.

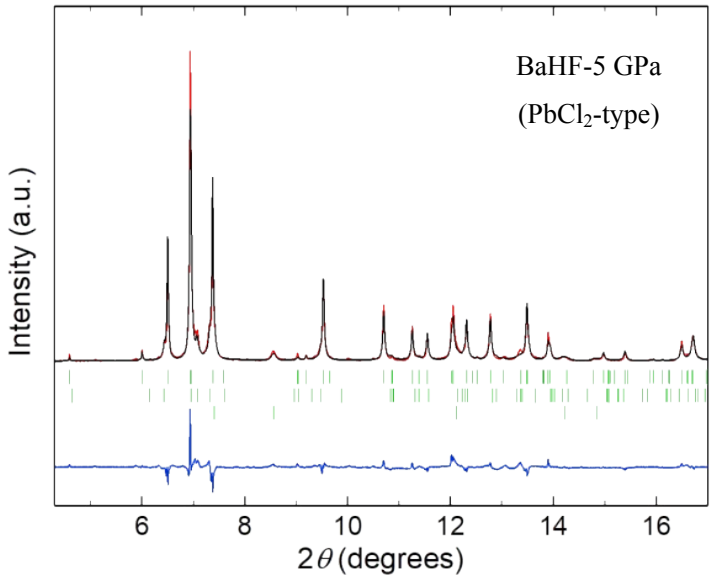

Figure S9. Rietveld refinement of SXRD data for BaHF synthesized at 5 GPa.

Table S8. Structural parameters of SXRD data for $PbCl_2$-type BaHF synthesized at 5 GPa.

atom	Wyckoff position	*x*	*y*	*z*	B_{iso} (Å^2)	*g*
Ba	4*c*	0.247(1)	0.25	0.113(2)	1.58(1)	1#
H1	4*c*	0.350(1)	0.25	0.440(1)	1#	0.244(3)**
H2	4*c*	0.978(2)	0.25	0.679(1)	1#	0.756(3)**
F1	4*c*	0.350(1)	0.25	0.440(1)	1#	0.756(3)**
F2	4*c*	0.978(2)	0.25	0.679(1)	1#	0.244(3)**

Space group *Pnma*; a = 6.8155(2) Å, b = 4.1095(2) Å, c = 7.8985(2) Å,

R_p = 9.26%, R_{wp} = 11.6%

**sum constrained to be 1, respectively.

#fixed to be 1.

Detailed description and results about First-principles calculations

Total energy calculations were performed using the projected-augmented planewave method (PAW) within parametrization of the exchange-correlation functional by generalized gradient approximation (GGA) and the Perdew−Burke−Ernzerhof (PBE) in Quantum ESPRESSO.[1-3] The cut-off energy is 80 Ry for all calculations and the *k*-point of *P*4/*nmm*, *Pnma*, *P*2*m*, and $P6_3/mmc$ SrHF models are respectively 3 × 3 × 3, 3 × 6 × 3, 3 × 3 × 6, and 9 × 9 × 6, which comply with the convergence criterion of 10^{-3} eV/atom by self-consistent calculations. A convergence threshold of 0.01 GPa was placed on the variable cells-relaxation (vc-relax) at zero temperature using Broyden–Fletcher–Goldfarb–Shanno (BFGS) quasi-newton algorithm with the maximum linear contraction of

the cell of 2.5.

The equilibrium structures of $PbCl_2$-type, anti-Fe_2P-type, and Ni_2In-type SrHF were built according to the corresponding reported structures, i.e., *Pnma*, *P*2*m*, and *P*6$_3$/*mmc* of SrH_2 and SrF_2,[4,5] but anion-ordered fluoride-type SrHF was built from reported LaHO (*P*4/*nmm*).[6] For each structure, two models were built with reverse anionic site occupancy, as shown in Figures S10, S11, S12, S13. After being geometrically optimized by vc-relax at p = 0 GPa and T = 0 K, these models (set as initial models) were subjected to different external pressure to obtain the total energy as a function of volume (Figure S14). The data ware fitted using the third-order Birch–Murnaghan isothermal equation of state,[7] and the calculated external pressure, the bulk modulus B_0, first-order pressure derivative B_0', and enthalpy were obtained (Table S9). The relative thermal stability of these phases was compared by their enthalpy values.

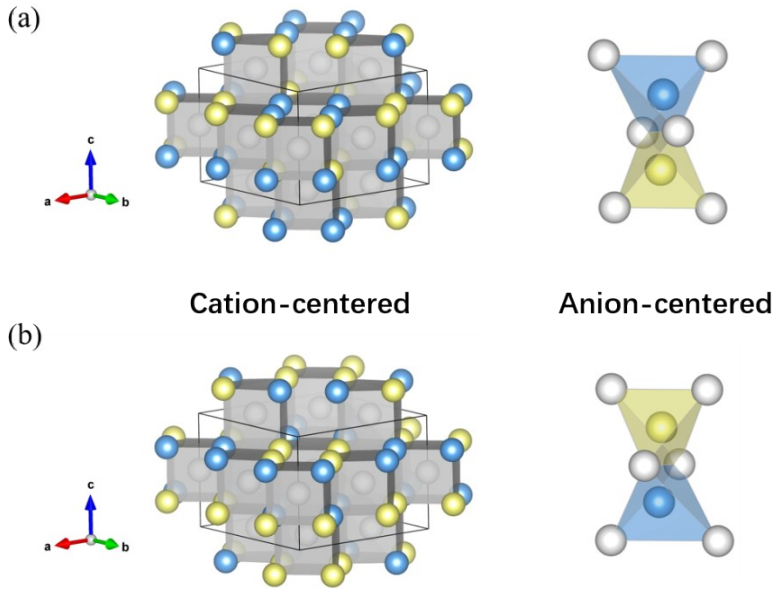

Figure S10. Crystal structures of fluorite-type (*Fm*-3*m*) SrHF with the coordination geometry around anions for (a) HSr_4-FSr_4 model and (b) swapped FSr_4-HSr_4 model. The right side of each panel represents a coordination environment around the anion center. White, blue, and yellow spheres denote Sr, H, and F atoms, respectively.

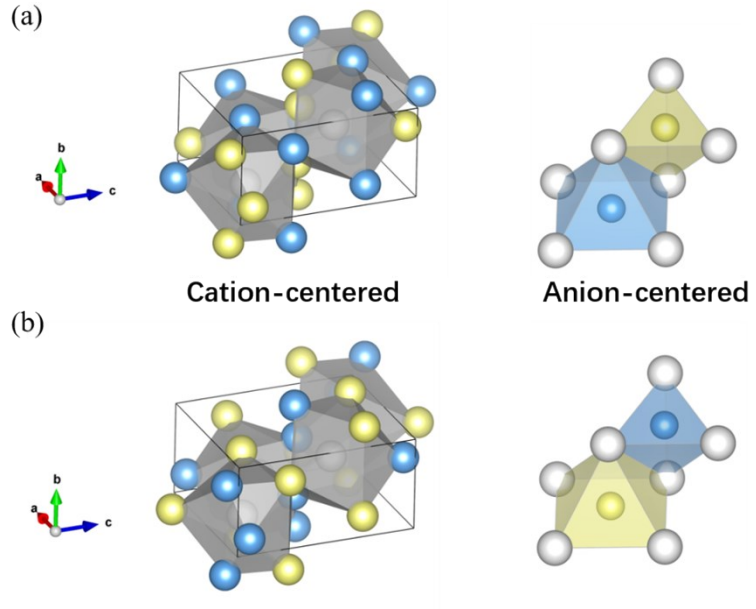

Figure S11. Crystal structures of $PbCl_2$-type (*Pnma*) SrHF with the coordination geometry around anions for (a) FSr_4-HSr_5 model and (b) HSr_4-FSr_5 model. The right side of each panel represents a coordination environment around the anion center. White, blue, and yellow spheres denote Sr, H, and F atoms, respectively.

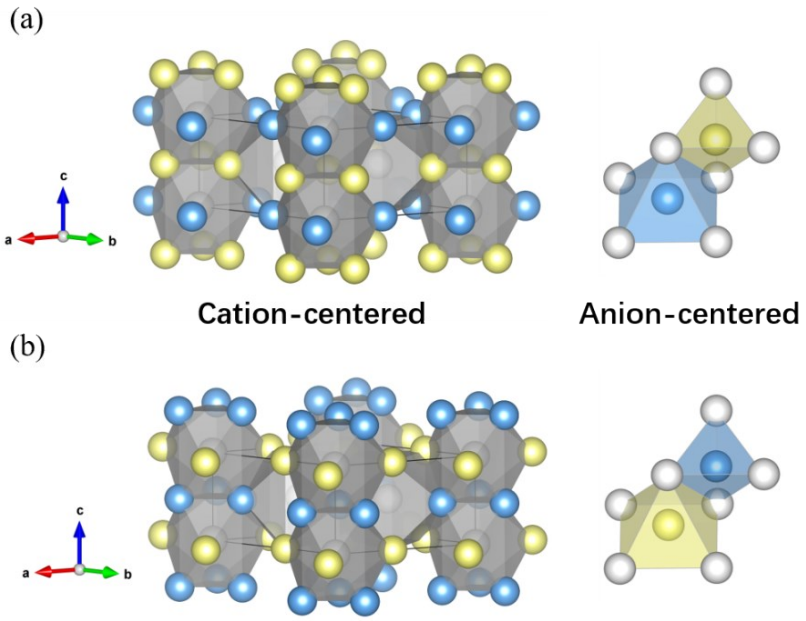

Figure S12. Crystal structures of anti-Fe_2P-type (*P*2*m*) SrHF with the coordination geometry around anions for (a) FSr_4-HSr_5 model and (b) HSr_4-FSr_5 model. The right side of each panel represents a coordination environment around the anion center. White, blue, and yellow spheres denote Sr, H, and F atoms, respectively.

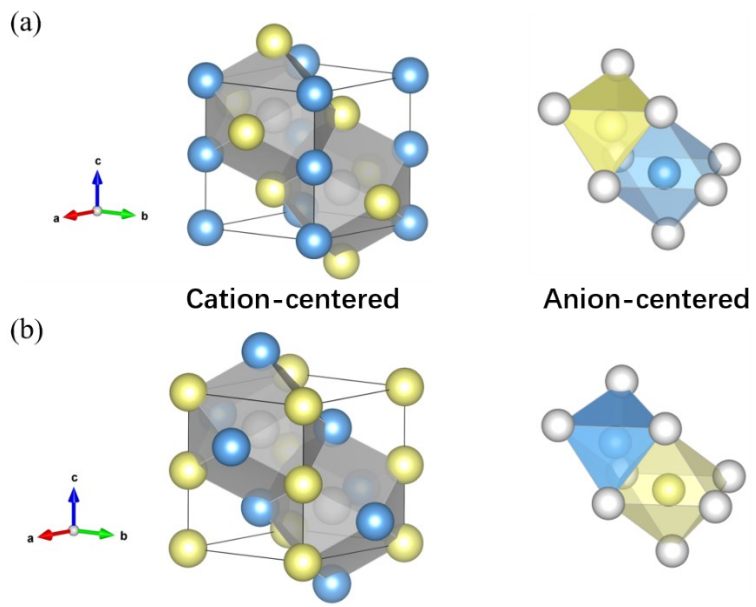

Figure S13. Crystal structures of Ni_2In-type ($P6_3/mmc$) SrHF with the coordination geometry around anions for (a) FSr_5-HSr_6 model and (b) HSr_5-FSr_6 model. The right side of each panel represents a coordination environment around the anion center. White, blue, and yellow spheres denote Sr, H, and F atoms, respectively.

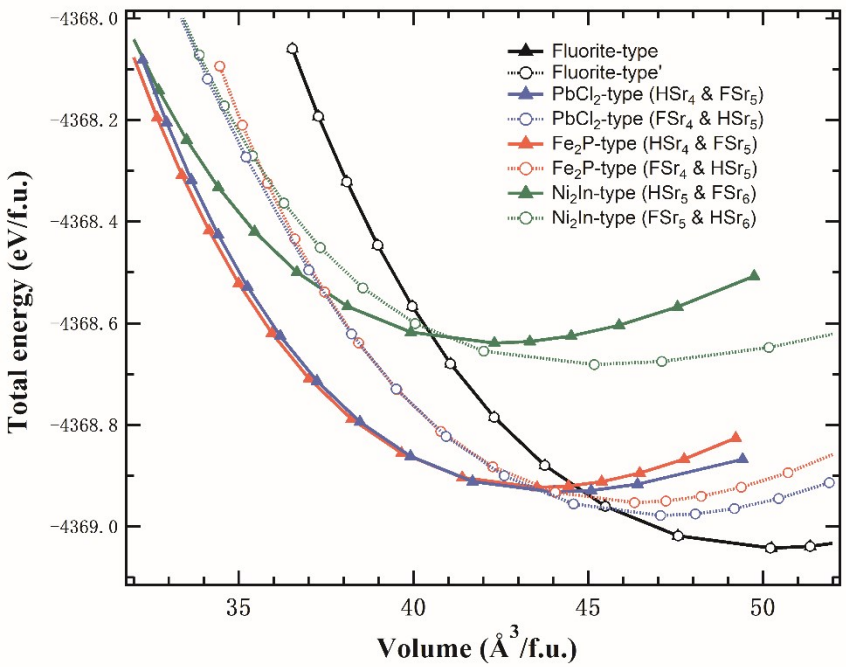

Figure S14. Total energy vs. volume relation for fluorite-type, $PbCl_2$-type, anti-Fe_2P-type, and Ni_2In-type SrHF.

Table S9. The fitting results of the third-order Birch–Murnaghan isothermal equation of state.

Model	Equilibrium Volume V_0 (Å^3/f.u.)	The bulk modulus B_0 (GPa)	B_0'
Fluorite-type (HSr_4-FSr_4)	50.254	48.4	4.43
Fluorite-type' (swapped FSr_4-HSr_4)	50.238	48.5	4.51
$PbCl_2$-type (HSr_4-FSr_5)	44.135	43.9	6.53
$PbCl_2$-type (FSr_4-HSr_5)	47.082	50.5	4.13
anti-Fe_2P-type (HSr_4-FSr_5)	43.570	52.7	4.27
anti-Fe_2P-type (FSr_4-HSr_5)	46.337	53.5	4.42
Ni_2In-type (HSr_5-FSr_6)	42.355	44.6	4.78
Ni_2In-type (FSr_6 -HSr_5)	45.725	29.5	6.05

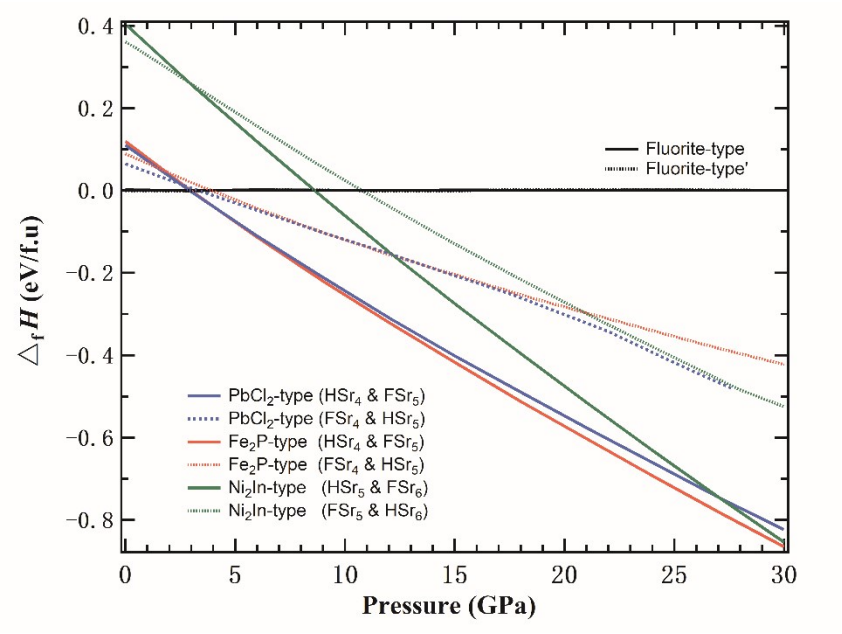

Figure S15. Calculated formation enthalpies as a function of pressure for $PbCl_2$-type, anti-Fe_2P-type, and Ni_2In-type SrHF, relative to fluorite-type SrHF.

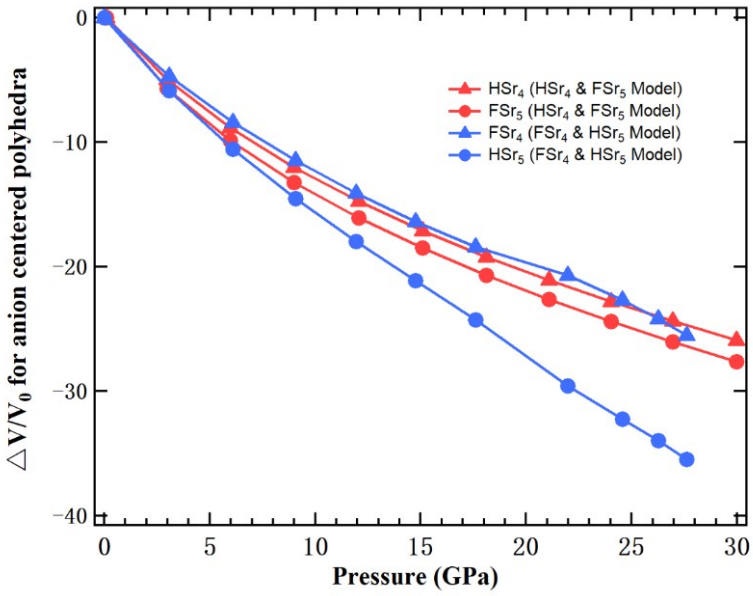

Figure S16. Calculated volume change of anion-centered polyhedra as a function of pressure for $PbCl_2$-type SrHF with FSr_4-HSr_5 model and HSr_4-FSr_5 model.

References

1. P. Giannozzi, S. Baroni, N. Bonini, M. Calandra, R. Car, C. Cavazzoni, D. Ceresoli, G. L. Chiarotti, M. Cococcioni, I. Dabo, A. Dal Corso, S. de Gironcoli, S. Fabris, G. Fratesi, R. Gebauer, U. Gerstmann, C. Gougoussis, A. Kokalj, M. Lazzeri, L. Martin-Samos, N. Marzari, F. Mauri, R. Mazzarello, S. Paolini, A. Pasquarello, L. Paulatto, C. Sbraccia, S. Scandolo, G. Sclauzero, A. P. Seitsonen, A. Smogunov, P. Umari and R. M. Wentzcovitch, *J. Phys. Condens. Matter*, 2009, **21**, 395502.
2. P. E. Blöchl, *Phys. Rev. B*, 1994, **50**, 17953–17979.
3. J. P. Perdew, A. Ruzsinszky, G. I. Csonka, O. A. Vydrov, G. E. Scuseria, L. A. Constantin, X. Zhou and K. Burke, *Phys. Rev. Lett.*, 2008, **100**, 136406.
4. J. S. Smith, S. Desgreniers, D. D. Klug and J. S. Tse, *Solid State Commun.*, 2009, **149**, 830–834.
5. J. S. Wang, C. L. Ma, D. Zhou, Y. S. Xu, M. Z. Zhang, W. Gao, H. Y. Zhu and Q. L. Cui, *J. Solid State Chem.*, 2012, **186**, 231–234.
6. H. Yamashita, T. Broux, Y. Kobayashi, F. Takeiri, H. Ubukata, T. Zhu, M. A. Hayward, K. Fujii, M. Yashima, K. Shitara, A. Kuwabara, T. Murakami and H. Kageyama, *J. Am. Chem. Soc.*, 2018, **140**, 11170–11173.
7. F. Birch, *J. Geophys. Res.*, 1978, **83**, 1257–1268.